

Extending Estimating Hydrogen Content in Atom Probe Tomography Experiments where H_2 Molecule Formation Occurs

Brief Title:

Extending Estimating Hydrogen Content in APT

Authors & Institutions:

Martin S Meier¹, Megan E Jones¹, Peter J Felfer², Michael P Moody¹, Daniel Haley¹

¹ *Department of Materials, University of Oxford, Parks Rd, Oxford, Oxfordshire OX1 3PH, UK*

² *Department of Materials Science and Engineering, Friedrich-Alexander-Universität Erlangen-Nürnberg, 91054 Erlangen, Germany*

Corresponding Author:

Martin S Meier, Materials Department, University of Oxford, 16 Parks Road, Oxford OX1 3PH, UK, Phone: +44 1865 2 83658, Fax: +44 1865 848790, Email: martin.meier@materials.ox.ac.uk

Abstract:

We investigate a new method for estimating specimen hydrogen content in Atom Probe Tomography (APT) in experiments where molecular hydrogen ions (H_2^+) originating from the measurement environment can overlap with deuterium (D^+) in the mass-to-charge-state spectrum, thus preventing direct application of isotopic marking for unambiguous hydrogen analysis. First, we apply an existing method for hydrogen content estimation, using H^+/H_2^+ ratios obtained from paired deuterated/non-deuterated experiments, demonstrating sufficient residual uncertainty to motivate exploring an alternative method to accurately estimate hydrogen content. By varying the time between evaporation events, it is then shown that a highly correlated relationship between field evaporation rate and hydrogen content can also be used to predict hydrogen content. This leads to a new method for measuring hydrogen content within the specimen. We combine this extrapolation technique with continuous cycling of the evaporation rate or pulse frequency during an APT experiment. This could enable spatially resolved imaging of hydrogen concentrations despite the presence of a contaminant background hydrogen signal, without the need for deuteration.

Keywords:

Hydrogen, Deuterium, Atom Probe Tomography, Hydrogen Peak Height Ratio, Evaporation Rate, Hydrogen/Deuterium Mass-to-Charge Spectrum Overlap

This is the accepted version.

Published version available in Microscopy&Microanalysis: doi.org/10.1017/S1431927621012332

1. Introduction

Hydrogen is a key element in many materials phenomena, such as hydrogen embrittlement in alloys (Robertson, et al., 2015) or hydride formation for hydrogen storage (Rusman & Dahari, 2016). However, characterisation of hydrogen at the atomic scale remains highly challenging. Whilst Atom Probe Tomography (APT) is in theory capable of imaging all elements with the same resolution and chemical sensitivity, and is therefore potentially well-suited for hydrogen imaging (Kesten, et al., 2002; Takahashi, et al., 2010), quantification of hydrogen remains difficult. One difficulty is that hydrogen and water vapour are primary residual gasses in vacuum chambers, leading to contaminant hydrogen in almost every APT experiment. Noise from these sources, when combined with low hydrogen concentrations in target materials, leads to signal-to-noise ratios that preclude direct quantitative analysis. Examples of such systems include hydrogen trapped at carbides in steel, where the number of hydrogen atoms might be well below 100 atoms per carbide (Takahashi, et al., 2010; Takahashi, et al., 2012; Haley, et al., 2014).

In several studies, this limitation was circumvented through the use of deuterium (Kesten, et al., 2002; Gemma, et al., 2009; Takahashi, et al., 2010; Chen, et al., 2017). The natural deuterium abundance is sufficiently low that its contribution to the background hydrogen signal in APT can be neglected - and any deuterium detected can be assumed to have originated from the sample. When the experimental parameters can be selected to maximise H^+ and minimise H_2^+ ion formation (Takahashi, et al., 2010; Chen, et al., 2017), deuteration allows for clear differentiation between contaminant and sample hydrogen effectively.

A key disadvantage of the method is that the high-field conditions in the APT experiment, where all contaminant hydrogen evaporates as H^+ ions, are typically only reached in voltage pulsed evaporation modes. When laser assisted evaporation is used, H_2^+ ions are commonly observed (Kellogg & Panitz, 1980; Sundell, et al., 2013; Kolli, 2017). In the case where deuterium containing samples are analysed, the formation of contaminant H_2^+ will occlude D^+ in the mass-to-charge-state-ratio spectrum (Figure 1) due to their similar ionic masses. Specifically, this overlap of H_2^+ and D^+ is rank-deficient. This means sample compositions cannot be computed with peak decomposition methods using adjacent peak heights and known isotopic abundances such as maximum-likelihood estimation (MLE) (London, 2019). It is however highly desirable in many cases to use laser assisted field evaporation, as it enables the analysis of non-conductive samples (Kellogg & Tsong, 1980), and higher analysis yields are obtained.

The ultimate limitation of this approach is that there are samples for which experiments cannot be reproduced with deuterium as a surrogate for naturally abundant hydrogen under lab conditions. As an example, this may be due to the involved timescales or sample histories not being clear, such as in geological samples (Reddy, et al., 2020) or in-service reactor components (Marian, et al., 2015).

In this work, we apply two methods for measuring hydrogen/deuterium contents in laser assisted field evaporation APT experiments. The first technique uses the comparison of mass-to-charge spectra collected before and after the samples are deuterium charged. This technique has been used before to demonstrate successful deuteration of APT tips (Haley, et al., 2014; Haley, et al., 2019; Breen, et al., 2020). The technique is believed to be accurate in settings where evaporation of H_2^+ ions can be fully suppressed, however, no accurate deuterium concentration in overlapped peaks has been calculated yet. The reasons for this were difficulties in estimating the ratio of H_2^+ and D^+ ions in the overlapped peak. We find that the ratios of contaminant H^+ and H_2^+ , and D^+ and D_2^+ ions from the sample do not agree, as will be subsequently shown. Ultimately, this places limits on the accuracy of deuterium content estimations that can be calculated with this method, demonstrating the need for an alternative.

The alternative technique which we propose in this study exploits the fact that there is a finite rate of supply of environmental hydrogen. Therefore, by changing the total ion flux onto the APT detector, the sample's true hydrogen content can be estimated statistically. We demonstrate a proof-of-concept to show that this method can reduce contaminant H^+ in composition estimations, using both multiple experiment and a novel rapid-cycling approach. The rapid cycling method may enable statistically resolved depth-profiling of hydrogen, without the need for isotopic labelling.

2. Theory

We summarise the fundamentals of the existing hydrogen estimation method based on peak height ratios, and introduce an alternative. The former, we term the “ratio method”. The alternative method, which tracks hydrogen levels with evaporation rate in order to provide a “true” hydrogen measurement, we term the “evaporation rate method”.

2.1 Ratio method

Deuterium tracer imaging methods, such as by Takahashi et al (Takahashi, et al., 2010), use a non-overlapping deuterium peak D^+ by applying conditions such that little-to-no H_2^+ is field evaporated. This ensures that H_2^+ ions in the $m/n = 2$ Da peak are negligible in deuterated experiments, and the peak can be uniquely assigned. Separately, a non-deuterated sample (hereinafter referred to as pre-run), can be used to demonstrate that H_2^+ is not observed. To limit sample-to-sample variability, and thus improve confidence in the absence of H_2^+ , this pre-run may be done on the same sample prior to deuterium-charging, making this a paired experiment.

In laser assisted APT experiments, where deuterium and hydrogen overlap considerably at $m/n = 2$ Da, further knowledge is needed to calculate the amount of deuterium $[D]$ in the sample. A laser evaporation pre-run is conducted and the ratio of counts in the background-corrected peaks $m/n = 1$ Da and 2 Da, i.e. the ratio H^+/H_2^+ , is measured. When the ratio H^+/H_2^+ is known, it is possible to apply a standard peak decomposition method to the (background corrected) $m/n = 2$ Da counts (n_2) in a subsequent experiment on a deuterated sample, in order to estimate the deuterium content. However, the key weakness in using this approach in laser mode is that the assumption that the ratios of H^+/H_2^+ and D^+/D_2^+ remain constant, which may not be the case.

Peak decomposition can be applied to a hydrogen-deuterium spectrum, as in Figure 1B, by two different methods. One method assumes H^+/H_2^+ has the same value for both contaminant hydrogen and deuterium from the sample. The $m/n = 1$ Da (H^+ , noise-corrected counts n_1) and $m/n = 4$ Da (D_2^+) are then used to solve the overlap at $m/n = 2$ Da. Alternatively, it is also possible to use the H^+/H_2^+ ratio and the $m/n = 1$ Da peak only to estimate the composition of the $m/n = 2$ Da peak. The number of deuterium ions at $m/n = 2$ Da (noise-corrected counts n_2) is then given by the following formula:

$$[D^+] = n_2 - n_1 * \left(\frac{[H_2^+]}{[H^+]} \right)_{prerun}$$

This approach assumes the H^+/H_2^+ ratio to be reasonably stable between experiments, which may be inaccurate (as will later be discussed, by means of Figure 2). Ratio changes may occur due to, for example, inhomogeneity in either chemistry or structure, or the electric field (Kellogg & Tsong, 1980; Sundell, et al., 2013). As such, we both explore the limitations of this ratio method, and further develop an additional approach based on time-varying detection rates.

2.2 Evaporation rate method

It has been reported that the amount of detected contaminant hydrogen in APT is approximately proportional to the inverse of pulsing rate (Sundell, et al., 2013; Kolli, 2017), indicating a supply effect. The inverse product of field evaporation rate r_{evp} and pulse frequency f_{pulse} is the (mean) time between evaporation events t_E . In turn, this time is proportional to the time available for contaminant hydrogen from the surrounding environment to arrive at the tip. If hydrogen supply is a dominant effect, changes in t_E should lead to changes in the observed amount of contaminant hydrogen. The field evaporation rate and the detection rate r_{det} , are related by the detection efficiency, making the set detection rate and frequency potential controls for contaminant hydrogen:

$$t_E = \frac{1}{f_{pulse} * r_{evp}} = \frac{1}{f_{pulse} * r_{det} * \zeta}$$

By changing the experimental conditions with time one can measure the hydrogen concentration H_{obs} , as a function of evaporation rate or pulse frequency. If the hydrogen supply is limited by the time available for hydrogen arrival and the true sample hydrogen concentration can be considered to be unaffected by the evaporation rate, then it is

theoretically possible to extrapolate the hydrogen concentration expected when there is zero time between evaporation events. In a laboratory context, this extrapolation corresponds to a theoretical measurement with infinitely high field evaporation rate. When the amount of contaminant hydrogen H_{cont} , is proportional to t_E , such an extrapolation should result in the observation of zero contaminant hydrogen. Consequently, we propose that the extrapolated concentration can predict the true amount of hydrogen originating from the sample H_{true} .

$$\lim_{t_E \rightarrow 0} H_{obs} = \lim_{t_E \rightarrow 0} (H_{true} + H_{cont}) = H_{true} + 0$$

Interestingly, as the evaporation rate and pulse frequency can be altered rapidly during an APT experiment, it is possible to perform this extrapolation within a single experiment. Requirements for this are a) a sufficiently wide range of evaporation rates or frequencies covered during the experiment, b) acquisition of sufficient ions at each evaporation rate or frequency and c) a sufficiently fast response to set-point changes in r_{evp} or f_{pulse} .

The detection rate, i.e. atoms detected per pulse, is an indirectly controlled parameter in APT, and maintained through control of the tip voltage. Thus, target and observed rates will differ. For this work, there is a key distinction between actual and target rate, as will be discussed subsequently. The pulse frequency is a directly controlled parameter, deviations between set-point and actual rate are expected to be negligibly small on modern machines, and changes can be made very rapidly. However, whilst changes of the target detection rate are possible on most APT machines, rapid changes in the pulse frequency are not widely supported (namely the Cameca LEAP 3000 HR machine in this study requires a warmup time after pulse frequency changes).

3. Materials and Methods

The sample material used in this study is a vanadium-carbide containing steel identical to the material studied by Chen et al. (Chen, et al., 2017), with nominal composition as given in Supplementary Material S1. This material was selected for three reasons. Firstly, this material has previously been used successfully for deuteration experiments in APT with electrochemical tip charging, indicating that deuterium tracing in such-prepared samples is feasible (Chen, et al., 2017; Chen, et al., 2019). Secondly, the material is known to provide some trapping sites for hydrogen, but not undergo any phase changes that would alter composition or structure significantly upon hydrogen uptake. Thirdly, steel samples typically give high experiment yield in APT, in both laser and voltage mode, and at high evaporation rate.

Specimens with dimensions of approximately 10 x 0.5 x 0.5 mm profile were cut from sheet. The samples were then electropolished in a manual two-step process, with rough stage using 25 % perchloric acid in acetic acid between 25 and 15 V and the fine step polishing using 2 % perchloric acid in butoxyethanol at 5 to 15 V.

For deuterium charging of the steel, the specimens were electrochemically charged, using a similar charging cell as described in (Haley, et al., 2014). The deuterium donating electrolyte was D₂O (99.9 %, AlfaAesar) with 0.1 M NaOH (> 97.5 %, BDH Laboratory Supplies) and 1 mmol HTMA (> 99.5 %, Sigma-Aldrich) (Al-Faqeer, et al., 2003). A gold wire is used as the counter electrode, a leakless Ag/AgCl electrode (Biochrom/Harvard apparatus) as the reference electrode, and the APT tip itself acts as the working electrode. A custom potentiometer was devised to hold the potential of the half-cell reaction at a constant 2.1 V for 30 s to charge the tips. Cryogenic transfer was conducted using our earlier protocol (Chen, et al., 2019). **Error! Reference source not found.** Table 1 and Table 2 provide an overview of the APT experiments that were conducted for this paper. For clarity, names have been assigned to the different experiment families and will be used in the following sections of this paper.

For determining the hydrogen/deuterium content via the ratio method described above, uncharged samples were analysed in a Cameca LEAP 3000 X HR in sequentially pulsed voltage and laser (532 nm wavelength) assisted evaporation modes until datasets of about 0.5 M to 1.5 M atoms (excluding surface contaminants) were acquired. These experiments are referred to as pre-runs. Voltage mode analysis conditions were 20 % pulse fraction, 200 kHz, 50K tip base temperature, and laser mode analysis conditions were either 0.2 nJ in Ratio-Low-Laser1, or 0.4 nJ in Ratio-High-Laser. The same samples were then charged with deuterium and re-analysed at the same experimental parameters to obtain data on the deuterated materials using voltage and laser assisted evaporation.

To extrapolate the hydrogen content from multiple measurements, a deuterated sample was analysed in laser assisted evaporation mode with a laser energy of 0.4 nJ a 60 K tip base temperature. The deuterated sample was analysed sequentially in three independent runs at 200 kHz pulse frequency and detection rates 1 %, 3.5 % and 7%, respectively. This family of experiments is referred to as Extrap-Manual. The LEAP 3000 XHR has a detection efficiency of 37 % (Martin, et al., 2017) hence the detection rates correspond to evaporation rates of approx. 2.7 %, 9.5 %, 18.9 %.

For determining the hydrogen content from a single APT experiment using automatic detection rate variation, non-deuterated samples were run at 40 pJ laser energy, 200 kHz pulsing rate, 40K tip base temperature. To cover a wide range of evaporation rates during the experiment, an AutoIT script (Jonathan Bennett & AutoIT Team, 2018) was used to cycle the target detection rate. Experiments with three different parameters were conducted. Two experiments in a LEAP 5000 XS2 atomprobe (laser wavelength: 355 nm) where the target evaporation rate was varied between 0.1 %, 1 % and 10 % (Extrap-Low-Rate), or between 3 %, 8 %, 12 % (Extrap-High-Rate) every 200,000 detected ions. The detection efficiency on the LEAP XS is approximately 80% (Prosa, et al., 2014), so the detection rates correspond to evaporation rates of 0.125 %, 1.25 %, 12.5 % (Extrap-Low-Rate) or 3.75 %, 10.0 %, 15 % (Extrap-High-Rate). In a third

¹ See *Table 2* **Error! Reference source not found.** for naming convention

² The LEAP 3000 X HR was decommissioned in summer 2019 and replaced by a LEAP 5000 XS, necessitating the use of different equipment for the two different measures.

experiment on a Cameca LEAP 5000 XR3 (laser wavelength 355 nm), the target detection rate was varied between 0.07 %, 0.7 %, 7 % every 500000 ions (Extrap-Few-Step, 50 K tip base temperature). The detection efficiency on this machine is 56%, so the evaporation rates are 0.125 %, 1.25 %, 12.5 %, making this run equivalent to Extrap-Low-Rate, but with less frequent changes in target detection rate.

To determine the hydrogen content from single APT tips using pulse frequency variation, a deuterated sample was run at 40 pJ laser energy, 50K tip base temperature and 1 % target detection rate in the Cameca LEAP XS machine. First, the pulse rate was switched between 125, 250, 333 kHz every 500000 ions (Extrap-Freq-Few-Step). After 15 M had been collected, the experiment was stopped and restarted, switching pulse rate every 150000 detection events (Extrap-Freq-Many-Step). An additional experiment (Extrap-Freq-High-Rate) was conducted on a non-deuterated tip (Cameca LEAP XR) with the same frequency cycling, switching every 500000 ions at a target detection rate of 5.6 %. The evaporation rates in these experiments correspond to the middle evaporation rates in the cycled evaporation rate experiments (1.25 % in Extrap-Freq-Few-Step and Extrap-Freq-Many-Step, corresponding to Extrap-Low-Rate, and 10 % in Extrap-Freq-High-Rate, corresponding to Extrap-High-Rate).

³ The LEAP 5000 XS in this study became unavailable due to technical failure, necessitating the use of a LEAP 5000 XR for one of the experiments with cycled evaporation rate

4. Results

4.1 Ratio method

The resulting mass-to-charge spectra of the same tips before and after deuteration in voltage and laser evaporation are shown in Figure 2. It is observed from Figure 2B and C that in non-deuterated tips, laser assisted evaporation leads to the appearance of an $m/n = 2$ Da peak. No such peaks are observed in the pulsed voltage experiments analysing the non-deuterated sample, as shown in Figure 2A. A clear $m/n = 2$ Da peak is visible in the pulsed voltage evaporation experiment on the deuterated sample (Figure 2A), but no $m/n = 3,4$ Da peaks are observed in the laser assisted evaporation experiments on the deuterated materials (Figure 2B and C). This absence of peaks at $m/n = 3,4$ Da is unexpected since the contaminant hydrogen is confirmed to form H_2^+ molecules in the laser pre-run. The counts in the $m/n = 1,2$ Da peaks and total collected and evaluated ions per measurement, all noise-corrected, are given in Table 2. Full mass-to-charge spectra are provided in the Supplementary Material S2, and voltage curves are included in Supplementary Material S3.

4.2 Evaporation rate method, manual experiments

As an alternative to estimating the hydrogen/deuterium content from peak height ratios, we investigate the feasibility of determining hydrogen contents through the extrapolation of a theoretical, infinitely fast experiment. As described in the section 2.2, the hydrogen contamination signal is expected to be proportional to the time between evaporation events t_E . In this section, we present the data that was obtained in subsequent APT experiments on the same tip at different evaporation rates (Extrap-Manual in **Table 2** **Error! Reference source not found.**).

Figure 3 plots the relative counts in $m/n = 1,2$ Da peaks in the Extrap-Manual experiment series, as function of t_E , after deuterium charging. As per the previous experiments, no $m/n = 3,4$ Da peaks representing HD^+ and D_2^+ are observed. While the extrapolated ionic concentration of the $m/n = 1$ Da peak is nearly zero (0.004 % at intercept), the extrapolated ionic concentration of $m/n = 2$ Da is 0.03 %.

Hydrogen was also observed to evaporate in the form of FeH^+ and FeH_2^+ ions, and their deuterium variants. FeH_2^+ and FeD^+ represent a mass-to-charge-state ratio overlap that, analogous to H_2^+/D^+ , cannot be directly decomposed. However, it is possible to calculate maximum likelihood estimates of the ionic concentrations of FeH^+ , FeD_2^+ and combined FeH_2^+ and FeD^+ . The results are shown in Figure 4. It is seen that all ion concentrations evolve with high linearity with the t_E (high R^2 values). The light hydrogen containing ions FeH^+ and the overlapped FeH_2^+/FeD^+ have small negative Y-axis intercepts (~ -0.1 %) and increase with t_E . In contrast to this, the FeD_2^+ concentration is nearly constant (line gradient nearly zero). It is noted that, as the iron-hydride/deuteride ions overlap with large Fe^+ peaks in the mass-to-charge spectrum, random scatter from these peaks may be carried into the calculated contents of iron hydrides/deuterides.

4.3 Evaporation rate method, automated experiments

The data points that are needed for a hydrogen content extrapolation do not need to be acquired in separate experiments. Instead, they can also be acquired in a single experiment by cycling the evaporation rate automatically. This potentially opens a route to probe the hydrogen behaviour spatially within the sample.

Three APT experiments on non-deuterated steel samples were conducted by repeatedly cycling the detection rate. The first experiment used a lower evaporation rate (Extrap-Low-Rate), cycling between 0.125 %, 1.25 % and 12.5 %, and the second a higher rate (Extrap-High-Rate), cycling between 3.75 %, 10 % and 15% target rate. In both cases, 200000 ions were collected at each target rate before the next target rate was set. The third experiment (Extrap-Few-Steps) uses the same evaporation rates as the first experiment, but with a wider step size of 500000 detector events.

In Figure 5 the observed detection rates and hydrogen detected during these experiments are shown. In Figure 5A (Extrap-Low-Rate), clear steps in the detection rate are visible. In Figure 5B (Extrap-High-Rate), the steps in the evaporation rate are less distinct, with especially the 10 % and 15 % target rate intervals merging into an almost continuous evaporation rate increase. This is due to the time required for the evaporation rate to reach set-point being longer than the time between step changes in the latter case. The evaporation rate cycling led to a “ripple” in the voltage curves of these experiments, as seen in Supplementary Material S3.

Table S5 in the supplementary material lists the observed detection and equivalent evaporation rates achieved for each target detection rate. The deviations between target and actual (observed) observed rates are attributed to the voltage control algorithm of the atom probe instruments used in this study. The voltage control algorithm behaves asymmetrically around the target rate, it ramps the voltage very conservatively when the actual rate is below target rate but drops the voltage quickly when above target rate. This explains why in both experiments with steps after 200000 ions (Extrap-Low-Rate and Extrap-High-Rate), the target and actual rate match reasonably well at the steps with lowest evaporation rate (0.125 % and 3.75 %) but not at the higher rates, where coming from a lower rate, the voltage is ramped up slowly. This can also be observed in the corresponding evaporation rate charts in Figure 5A and B. The Extrap-Few-Step experiment with less frequent steps is less affected, as there is more time for voltage adjustments between target detection rate changes. Direct control of the voltage through the rate cycling script could be a potential solution to this problem.

The datasets were sectioned along the steps in the evaporation rate, such that each dataset yielded three derived datasets with different evaporation rates. For each derived dataset, the hydrogen content is calculated for every evaporation rate. The extrapolated hydrogen contents for these nominally hydrogen-free samples are shown in Figure 6 (Extrap-Low-Rate, Extrap-High-Rate) and Figure 7 (Extrap-Few-Step). For Extrap-Few-Step in Figure 7, three variants of this extrapolation were conducted, using the entire dataset (Figure 7A), only the first 100000 detector events after each change in target evaporation rate (Figure 7B), and only the last 100000 detector events before each change in target evaporation rate (Figure 7C). These sections of 100000 events are also indicated on the horizontal axes in Figure 5C.

As described in Section 2.2, two experiments with cycled pulse frequency were conducted on a deuterated tip, Extrap-Freq-Few-Step and Extrap-Freq-Many-Step. The evolution of hydrogen with the pulse frequency in these experiments is shown in Supplementary Material S6. A small partial fracture occurred in Extrap-Freq-Many-Step as seen in the voltage curve in Supplementary Material S3, however this has not interrupted the cycling or the course of the experiment. A third experiment at higher target detection rate (5.6 %), Extrap-Freq-High-Rate, was conducted on a non-deuterated tip. The hydrogen evolution of this experiment is shown in Supplementary Material S6 C. Similar to the experiments with cycled evaporation rate, the datasets are sliced along changes in the pulse frequency to yield three derived datasets. The ionic amount of hydrogen for each of these datasets are plotted as function of time between evaporation events, and extrapolated to an infinitely fast experiment (Figure 8).

In all these experiments, both evaporation rate and pulse frequency cycled, the sum of hydrogen from the three peaks $m/n = 1,2,3$ Da evolves linearly ($R^2 > 0.95$) with t_E . An extrapolation to infinitely fast experiments in the varied evaporation rate experiments leads to a combined H^+, H_2^+, H_3^+ ionic content of approximately 3.4 % in the low-rate extrapolation experiment (Extrap-Low-Rate) and 0.2 % in the high-rate experiment (Extrap-High-Rate). The extrapolated ionic contents of hydrogen in the cycled frequency experiments are 0.35 % (Extrap-Freq-Few-Step), 0.7 % (Extrap-Freq-Many-Step) and 0.04 % (Extrap-Freq-High-Rate).

A low number of H_3^+ ions were observed in in the low-rate cycled evaporation rate (Extrap-Low-Rate) and few steps cycled frequency experiment (Extrap-Freq-Few-Step), but not in any other experiment in this paper. Moreover, a $m/n=4$ peak, corresponding to D_2^+ was found in Extrap-Freq-Few-Step, however these are distinctly segregated to surface on the tip of the specimen. This suggests these rather originate from surface adsorbates or a potential oxide layer, but not the actual sample material. The hydrogen spectra for all cycled rate and frequency experiments are provided in Supplementary Material S3.

5. Discussion

5.1 Ratio method

First, we discuss the results of the paired non-deuterated (pre-runs) and deuterated datasets in the ratio experiments (Ratio-Low-Laser and Ratio-High-Laser). In the pulsed voltage evaporation experiments, a $m/n = 1$ Da peak in the voltage-mode pre-run is observed due to H^+ ions, but no H_2^+ molecules were detected (no peak at $m/n = 2$ Da). The peak observed at $m/n = 2$ Da after deuteration is therefore due to D^+ only, demonstrating successful deuteration (Figure 2A, Table 2). In the laser evaporation experiments in Ratio-Low-Laser and Ratio-High-Laser (Figure 2B and C, Table 2), peaks at $m/n = 1, 2$ Da are observed in the non-deuterated runs due to H_2^+ evaporating besides of H^+ . If hydrogen and deuterium evaporate in the same H^+/H_2^+ ratio, then D_2^+ and HD^+ from the deuterated tip should appear at $m/n = 3, 4$ Da. As seen in Figure 2B and C, this is not observed in the spectra. A decomposition of the $m/n = 2$ Da peak based and the peaks at $m/n = 1$ and 4 Da is therefore not possible in this case.

Table 2 shows that the ratio of the peaks at $m/n = 1, 2$ Da in laser mode have changed after deuteration, with the $m/n = 2$ Da peak relatively higher, presumably due to D^+ ions. This indicates that light and heavy hydrogen in the sample do not evaporate as dimer ions with the same ratio. The spectra show that the formation rate of D_2^+ molecules is zero or negligibly low at the experimental conditions, but this is not the case for H_2^+ molecules.

It is noted that the absence of the $m/n = 4$ Da peak is a significant observation. If the ratios of H^+ to H_2^+ for sample deuterium and contaminant hydrogen were the same, peaks of certain heights above the noise background are expected at $m/n = 4$ Da in the deuterated laser evaporation experiments. These expected counts above noise floor at the $m/n = 4$ Da peak are listed in Table 4. In order to obtain an estimate of the noise floor at $m/n = 4$ Da, the background around this region is fitted with a constant TOF background (Intervals [$m/n = 2.7-3.5, 4.5-5.5$]), and the expected background counts are calculated. It is seen that the fitted background predicts the measured counts at $m/n = 4$ Da very well. This indicates that no or very few real detector events are detected at $m/n = 4$ Da. The expected counts above the noise floor are significantly higher than the measured deviations. Thus, uncertainty due to the noise cannot account for the missing $m/n = 4$ Da peak.

The reason for the different behaviour of H and D is believed to be the state in which these species are present on the sample. Contaminant hydrogen arrives as molecules at the sample surface and is most likely at least partly contained in adsorbed molecules ($H_{2,ads}, H_2O_{ads}$). Deuterium on the other hand has been absorbed into the metal matrix during charging, or is sitting in traps at the carbides or elsewhere in the material. In this state, deuterium may be clustered, but not grouped into such molecules. Molecular evaporation of sample hydrogen therefore requires additional steps of reaction and eventual diffusion. These recombination reactions are not guaranteed to occur (as in this study), and in instances where they are occurring, the rates of sample hydrogen molecule formation cannot be predicted from observations on contaminant hydrogen molecule evaporation.

Without the peak at $m/n = 4$ Da, it is still possible to assume that the H^+/H_2^+ ratios from the pre-run are reasonably stable compared to the deuterated experiments, as described in Section 2.1. The peak ratios derived from Table 3 and the resulting ionic deuterium content estimates are listed in Table 5. For comparison, the D^+ amounts in the voltage evaporation runs, where the $m/n = 2$ Da peak is not overlapped are listed as well.

It is seen that the decomposed D^+ contents (0.023 %, 0.034 %, Table 5) in laser evaporation experiments lie between the two concentrations measured in the voltage experiments (0.009 %, 0.046 %, Table 5). On the other hand, the relative deviations between the decomposed D^+ contents for laser mode and the D^+ contents measured in voltage evaporation are high (+252 % and -74 %). The total amounts of deuterium in the material are low, as expected for steel. It is therefore difficult to ascertain how accurately the calculated D^+ contents resemble the actual ionic content in the sample, ultimately limiting the utility of peak ratio methods in laser mode.

Possible sources of error could be variations in the H^+/H_2^+ between pre-run and deuterated laser mode run, and evaporation of deuterium in complex molecules. As the deuterated voltage and laser evaporation runs for both samples are paired, it is expected that the deuterium contents in these experiments are very similar. However,

eventual differences in actual deuterium content between voltage and laser mode runs cannot be ruled out or quantified from this data. This complicates the assessment of the accuracy of deuterium content estimates.

It has also been shown that changes in the electric field (or tip voltage) during the experiment can influence the H^+/H_2^+ ratio (Kellogg & Tsong, 1980; Sundell, et al., 2013). The ratio method as used here does not account for changes in the ratio due to the field, which means that electric field differences between pre- and deuterated runs might be biased. To the author's knowledge, it is currently not known to what extent changes in the H^+/H_2^+ ratio can be attributed to electric field changes.

To conclude, the reliability of the ratio method for hydrogen content measurement is hampered by several issues. These include uncertainties about H^+/H_2^+ ratio variations due to field changes or other factors, and, disconcertingly, different H^+/H_2^+ ratios for contaminant and sample hydrogen, as indicated by the missing D_2^+ peak at $m/n=4$ in this study. Therefore, the authors believe that the ratio method is not an ideal hydrogen content estimation method in cases where H_2^+ molecules may evaporate, and recommend exploring alternatives when quantitative measurements are needed.

5.2 Evaporation rate method, manual experiments

The following section discusses the applicability and accuracy of the approach for suppressing the contribution of contaminant hydrogen by controlling the time available for hydrogen arrival by varying the detection rate. Unlike the previously discussed approach of using peak ratios for decomposition, this approach can allow for deuterium content estimations without knowledge of peak ratios.

The ionic concentrations of peaks $m/n=1,2$ Da as function of time between evaporation events (t_E) are plotted in Figure 3. It is seen that the straight line fit to the data shows high R^2 values of 0.9996 ($m/n = 1$ Da) and 0.914 ($m/n = 2$ Da) (Figure 3), indicating that a linear model explains the variation relatively well. This shows firstly that within the boundaries of this experiment, the amount of detected contaminant hydrogen in $m/n = 1$ Da scales linearly with t_E . Secondly, it demonstrates that the extrapolation technique in our experiments can be used to successfully suppress the contribution of contaminant hydrogen signal in this peak.

The $m/n = 2$ Da peak is different in that the extrapolation does not lead to a content of zero, but rather 0.03 %. This can be explained by the presence of D^+ ions. Specifically, unlike the contaminant H_2^+ , D^+ is independent of the evaporation rate and does not disappear at infinitely fast evaporation.

It is noted that the counts at $m/n = 2$ Da do not follow as perfectly a linear relationship, but still have high R^2 (Figure 3). It is also noted that even when excluding the highest evaporation rate (data point with lowest t_E) from the extrapolation, the resulting content in $m/n = 2$ Da is still nonzero (0.013 %). This is clearly above the 0.004 % extrapolated for $m/n = 1$ Da. Thus, the conclusion does not change even when regarding this specific point as an outlier.

Since the deuterium is trapped at lattice defects/carbides in this material (Krom & Bakker, 2000; Takahashi, et al., 2012), spatial inhomogeneity could contribute to the observed deviation in the apparent deuterium concentration. It is also known that the H^+/H_2^+ ratio in APT generally varies with the electric field strength at which the evaporation occurs (Kellogg & Tsong, 1980; Sundell, et al., 2013), which may be another contributing factor to the observed deviation.

The deuterium contents in this material are low when compared to the amount of contaminant hydrogen (0.009 % and 0.045 % deuterium content are measured in voltage mode evaporation for the material in this paper, as seen in Table 5). Nevertheless, the authors are confident that the extrapolated value of 0.03 % represents a reasonable estimate of the deuterium for two reasons. Firstly, the contaminant H^+ concentration scales highly linear with the evaporation rate ($R^2 = 0.9996$), which is unlikely to be the result of a random coincidence. Secondly, even higher linearities are reproduced in the cycled evaporation rate experiment Extrap-High-Rate, which used a similar range of evaporation rates (Sections 4.3, 5.3, $R^2 > 0.9999$). This means that the high linearity and H^+ suppression is seen on distinct instruments (LEAP 5000 XS and 3000 XHR), for distinct tip base temperatures (40 K instead of 60 K), and

independent of cycling method (quickly varying instead of static evaporation rate). The combination of all these factors having very limited effect on the linearity makes errors arising from higher-order effects like dissociation of complex ions unlikely. It is however noted that some variability in the extrapolated hydrogen amount linked to the depth is observed, as will be discussed in Section 5.5.

The Fe-hydride ions in steel (Figure 4) show a trend that is consistent with the detection of contaminant hydrogen and deuterium at $m/n = 1,2$ Da. Other than FeH^+ and combined FeH_2^+/FeD , the FeD_2^+ ionic concentration is not influenced by contaminant hydrogen arriving during the experiment and therefore evaporation rate independent. This indicates that the Fe-hydride ions do not transport relevant quantities of contaminant hydrogen at (theoretical) infinite evaporation rates. In particular, this means that the observed suppression of contaminant hydrogen in Figure 3 is not the result of an overlooked shift in hydrogen evaporation towards complex molecules at high evaporation rates. Instead, it is better explained as a rate-limited phenomenon, consistent with H^+ and H_2^+ .

5.3 Evaporation rate method, automated experiments

Like in the extrapolations from discrete experiments, the detected hydrogen contents scale linearly with t_E . It is however observed that only the high-rate extrapolation run (Extrap-High-Rate) approximately yielded the expected extrapolated hydrogen signal of 0. The low-rate extrapolation run (Extrap-Low-Rate) resulted in approximately 3.4 ionic-% combined H^+ , H_2^+ and H_3^+ . It seems unlikely that this value reflects a correctly measured hydrogen content, as it is far above hydrogen contents that are typically reached in steels (Takahashi, et al., 2018; Liu, et al., 2019), and also far above deuterium contents measured in the deuterated voltage evaporation experiments in this paper (0.009 % and 0.045 %, Table 5). Figure 6A reveals that this is due to the H^+ ions, which do not follow the linear trend as closely as the other species, resulting in estimation error.

A possible factor that contributes to this error can be found in the evolution of the hydrogen content in Figure 5. It is seen in Figure 5A that in the low-rate extrapolation run (Extrap-Low-Rate), the evaporation rate is stable when the target evaporation rate is set to 0.125 % (equivalent detection rate 0.1 %). When the target rate is switched to the higher levels 1.25 % or 12.5 %, the evaporation rate stabilises at certain higher levels after a ramp. Such a stabilisation is however not observed in the H^+ rate, which appears to react in a much more ‘sluggish’ way, not reaching a stable value but rather gradually tailing off during the steps where the target evaporation rate is 1.25 % or 12.5 %. This is also in sharp contrast to the H_2^+ rate, which does not tail off like H^+ , but reacts promptly to changes in the evaporation rate.

From this, it may be inferred that a significant proportion of all detected H^+ ions is the result of a different mechanism than the evaporation of H_2^+ ions. One possible explanation could be that the evaporation of H^+ ions is tied to the presence of certain species at the sample surface, and that a reservoir of these species gradually builds up during evaporation at a low rate and gradually decreases in extent as the evaporation rate is set to higher values. No hints to such a reservoir would be observed for H_2^+ as it promptly reacts to evaporation rate changes. Instead, H_2^+ might rather originate from a short-lived species at the sample surface.

The experiment with less frequent steps in evaporation rate (Extrap-Few-Step) adds further support to this hypothesis. A slow tail-off of H^+ ions, similar to Figure 5A, is seen in Figure 5C, but unlike Figure 5A, the steps in target evaporation rate are sufficiently spaced out such that the hydrogen content equilibrates. Thus, any “transition” regions can be excluded to obtain a “stable” hydrogen extrapolation. This result is seen in Figure 7C, where extrapolation was conducted only on the 100000 detector events collected prior to target evaporation rate changes. The opposite is to extrapolate using only “transition” phase data collected directly after changes in evaporation rate. This is done in Figure 7B where only the first 100000 detector events after changes in evaporation rate were used (see rectangles at horizontal axes in Figure 5C for how the dataset was sliced). It is clearly seen that the stable hydrogen detection in Figure 7C scales much more linearly with t_E than transition hydrogen detection in Figure 7B. However, it is noted that even the extrapolation on stable hydrogen in Figure 7C leads to hydrogen content of 2.2 %, which is too high for steel. It is therefore concluded that there may be additional factors that lead to reduced accuracy in hydrogen content extrapolations in cycled evaporation rate experiments, where steps with very low evaporation rate are used.

No similarly obvious tail-off in any hydrogen species is observed in the high-rate extrapolation run (Extrap-High-Rate) in Figure 5B. The authors attribute this to the absence of steps with very low evaporation rates in this experiment. These steps have led to very high amounts of contaminant hydrogen in the other cycled rate experiments (>20 % in Extrap-Low-Rate, > 9 % in Extrap-Few-Step). It is speculated that some higher-order effects are more pronounced when the concentration of contaminant hydrogen reaches values similar to the concentration of sample ions in the spectrum. Thus, avoiding such evaporation rates could have led to the better extrapolation result in Extrap-High-Rate. It is however also noted that the steps in the evaporation rate are less clear in this experiment, and the transition from 3.75 % to 10 % to 15 % evaporation rate are rather continuous ramps. The visual identification of tail-offs in the diagram is therefore in general more difficult in this experiment.

One potential source of error that needs to be considered in experiments with cycled evaporation rate is the effect of the electric field. It has been shown (Kellogg, 1981; Sundell, et al., 2013) that changes in the electric field during an experiment influence the amount of detected contaminant hydrogen. In detection-rate controlled APT experiments, changes in the evaporation rate are achieved through adjustments of the DC voltage (Tsong, 1978). Thus, if the electric field is systematically different during phases with different evaporation rate, an error could be possible.

The charge state ratio (CSR) of Fe-56 ions can be used as a measure for the electric field in the steel specimen used for this study (Supplementary Material S7). In Extrap-Low-Rate, the CSR for the three evaporation rates are very distinct, indicating different electric fields. This is different in the Extrap-High-Rate experiments, where the CSRs between the evaporation rates are much more similar, indicating minimal change, and thus influence of the electric field on the contaminant hydrogen. It is therefore believed that the electric field has not critically influenced the results in Extrap-High-Rate. Furthermore, results similar to Extrap-High-Rate are obtained in the cycled frequency experiments (Section 5.4), which are not, or to a much lesser extent, affected by such field changes.

5.4 Pulse frequency method, automated experiments

To minimise concerns that observed changes in hydrogen are due to changes in the voltage required to achieve certain evaporation rates, we also applied frequency cycling. The extrapolations in Figure 8 show that the high linearities of the extrapolations persist in this cycling mode, and the amount of contaminant hydrogen continues to extrapolate to near zero. Other than in the cycled evaporation experiments, only a minor (Extrap-Freq-Few-Step and Extrap-Freq-Many-Step) or no (Extrap-Freq-High-Rate) difference in charge state ratios upon frequency changes is detected in these experiments, as seen in Supplementary Material S7. This eliminates the electric field as a potential source of error or uncertainty.

The slow tail-offs of H^+ , observed in Extrap-Low-Rate are also found in Extrap-Freq-Few-Step and Extrap-Freq-Many-Step. The extrapolation diagram for Extrap-Freq-Low-Step (Figure 8A) also shows a deviation from the ideal linear behaviour, similar to Extrap-Low-Rate, where this was attributed to the tail-off of H^+ . No such deviation is seen in Extrap-Freq-Many-Step (Figure 8B), despite identical experimental parameters, except from the smaller step width of 150000 compared to 500000. The authors believe the small step size in Extrap-Freq-Many-Step has led to a smearing out of the slower response of H^+ to frequency changes across all steps. No such observations of tail-offs are made in Extrap-Freq-High-Rate (Figure 8C), in agreement with Extrap-High-Rate. Furthermore, H_2^+ seems to not be affected by a sluggish response to frequency changes, also agreeing with the observations on the cycled evaporation rate experiments (Section 5.3).

In contrast to the experiments with stepped evaporation rate and Extrap-Freq-High-Rate, the data in Extrap-Freq-Few-Step and Extrap-Freq-Many-Step was collected on a deuterated tip. The extrapolated amounts of the $m/n = 2$ Da peaks, which in these samples contain D^+ as well as contaminant H_2^+ , extrapolate to 0.015 % (Extrap-Freq-Few-Step, Figure 8A) and 0.036 % (Extrap-Freq-Many-Step, Figure 8B). This is above the extrapolated amount of H_2^+ in the non-deuterated Extrap-Freq-High-Rate (0.0071 %, Figure 8C). This could indicate that deuterium was successfully measured in these experiments. However, there is uncertainty about this, as no repetitions of the experiments were conducted

and sources of error like potential reservoirs of contaminant hydrogen might exist. More research and comparisons with other materials will be needed to assess the reliability and accuracy of the method. It is noted that the extrapolation technique in general does not require samples to be deuterated for a detection of sample hydrogen, as both contaminant H^+ and H_2^+ reliably extrapolate to (near) zero.

5.5 Potential Depth-Profiling using Cycled Rates

In principle, the cycled evaporation rate technique may enable depth profiling and eventually fully 3D spatial imaging of hydrogen concentrations in APT samples. To explore this, we apply two different methods for conducting localised hydrogen extrapolation, layer-based for depth estimation and voxel-based for 3D estimation.

For the layer-based method, the datasets were sliced along the changes in evaporation rate or frequency, resulting in curved layers in reconstruction space. Extrapolation is conducted for each layer using values obtained from the neighbouring layers and the current layer itself. The detected amounts of hydrogen for each layer are shown in Supplementary Material S8 and S9, and the extrapolated amounts are shown in Figure 9. While the amounts of detected hydrogen - both H^+ and H_2^+ - increase throughout all experiments with increasing depth, the extrapolated amounts, in particular H_2^+ , show a more varied behaviour. It is notable that the amount of extrapolated H^+ at least slightly increases with increasing depth in all of the experiments. The authors do not know what the cause of this phenomenon could be. More research is needed to explain this increase, which may either be real or an artefact.

In Extrap-Freq-High-Rate (Figure 9D), the amount of extrapolated contaminant hydrogen for all layers is below 0.08 %. This indicates that, with a careful selection of parameters, depth profiling could be feasible if the hydrogen concentration difference exceeds approximately 0.1 % under optimal circumstances. In this study, deuterium contents of 0.009 % (Ratio-Low-Laser) and 0.046 % (Ratio-High-Laser) were found in deuterated samples of the steel using pulsed voltage evaporation. This concentration range suggests that depth profiling in this material could be possible, but challenging.

Finally, we demonstrate a voxel-based extrapolation method as a potential method of extrapolating hydrogen with a full 3D resolution. For this method, a “very” local evaporation rate and concentration for every hydrogen detection is calculated based on detection events before and after every hydrogen detection. The dataset is then sliced into voxels, and extrapolation is conducted for every voxel using the hydrogen ions contained within these voxels.

Figure 10 shows 10nm slices along and perpendicular to the tip direction of the extrapolated amounts of hydrogen in Extrap-Freq-High-Rate. It is seen that the amount of H^+ at the top of the tip is increased, which could indicate the presence of surface oxides. However, no clear co-segregation of the extrapolated hydrogen with the carbides in the sample is seen, likely as concentrations are too low to permit full 3D analysis. The results of a voxel-based extrapolation of Extrap-Low-Rate (Supplementary Material S10) on the other hand show certain structures, resembling patterns from pole segregation. This is unique to this experiment and has not been observed in any other dataset in this study.

6. Summary & Conclusion

Our work investigates two techniques for estimating the hydrogen content from APT laser mode experiments. The first technique uses H_2^+ molecule formation rates from a paired uncharged experiment prior to deuteration. This approach was found to be inaccurate as molecule evaporation ratios for contaminant and sample hydrogen are too dissimilar. Using only the $m/n = 1$ Da peak and pre-run H^+/H_2^+ ratio, it was possible to estimate D^+ contents in deuterated runs with overlapped $m/n = 2$ Da peaks. The obtained values lie in the range expected from the pulsed voltage evaporation experiments. However, uncertainty about the accuracy of the results remains. This motivates the search for an alternative method.

The second technique was via the extrapolation of the hydrogen content measured at different evaporation rates or frequencies. Under the assumption that the hydrogen contamination is time dependant, zero or near-zero contaminant hydrogen is expected as the evaporation rate tends to infinity. This was applied to extrapolate hydrogen from both sequential experiments, and automated experiments which rapidly cycle the evaporation rate or frequency.

It was found that contaminant hydrogen scales nearly linearly with the time between evaporation events (t_E), and contaminant hydrogen drops near zero as the experiment approaches infinite evaporation rate or frequency. Furthermore, there may be a saturation limit, as when using low detection rates (0.1 %) this led to higher estimates of H content. This is potentially due to the build-up of a reservoir of H^+ evaporating species at low evaporation rates. This effect could limit depth resolution and accuracy until an improved model of the dynamics of the surface hydrogen is available.

Cycling the frequency or evaporation rate during an experiment is a new method to estimate hydrogen content from within samples, which does not require deuteration of the material. Localised extrapolation allows spatial location of the hydrogen in the material, but scatter and artefacts are still problematic. Further research is needed to increase the sensitivity to achieve full spatial localisation but remains a promising research avenue.

In the analyses of hydrogen in APT, it has often been assumed that the contribution of contaminant hydrogen becomes negligible in samples where the absolute measured concentration of hydrogen is sufficiently large, such that at least approximate measurements of concentrations become possible. The nearly perfectly linear scaling of the amount of detected contaminant hydrogen with time between evaporation events suggests that this is inaccurate. Instead, it indicates that the experimental conditions strongly influence the amount of detected hydrogen. The authors therefore recommend analysis of the evaporation rate or pulse frequency dependence of hydrogen detection, or other verification methods to be applied in studies on such materials.

7. Data Accessibility Statement

The raw data as well as reconstructed APT datasets from this paper are available on the Oxford Research Archive ORA: <https://ora.ox.ac.uk/objects/uuid:2b504432-0b45-42f5-8bfa-9d0ad5a6a64f>. Additionally, the authors will provide the data upon request.

8. Acknowledgements

The authors would like to thank P Gong and W M Rainforth from the University of Sheffield for supplying the sample material. M S Meier acknowledges support from Cameca Instruments. M E Jones acknowledges support from EPSRC, Rolls Royce Plc. and National Nuclear Laboratory. D Haley acknowledges EPSRC funding from EP/P001645/1 Advanced Nuclear Materials. P. Felfer has received funding from the European Research Council (ERC) under the European Union's Horizon 2020 research and innovation programme, (Grant agreement No. 085065).

9. References

- AL-FAQEER, F.M., WEIL, K.G. & PICKERING, H.W. (2003). Analysis of hydrogen absorption under competitive adsorption conditions - Effect of hexamethylenetetramine. *Journal of the Electrochemical Society* **150**(5), B211-B216.
- BREEN, A.J., STEPHENSON, L.T., SUN, B., LI, Y., KASIAN, O., RAABE, D., HERBIG, M. & GAULT, B. (2020). Solute hydrogen and deuterium observed at the near atomic scale in high-strength steel. *Acta Materialia* **188**, 108-120.
- CHEN, Y.-S., BAGOT, P.A.J., MOODY, M.P. & HALEY, D. (2019). Observing hydrogen in steel using cryogenic atom probe tomography: A simplified approach. *International Journal of Hydrogen Energy* **44**(60), 32280-32291.
- CHEN, Y.-S., HALEY, D., GERSTL, S.S.A., LONDON, A.J., SWEENEY, F., WEPF, R.A., RAINFORTH, W.M., BAGOT, P.A.J. & MOODY, M.P. (2017). Direct observation of individual hydrogen atoms at trapping sites in a ferritic steel. *Science* **355**(6330), 1196-1199.
- GEMMA, R., AL-KASSAB, T., KIRCHHEIM, R. & PUNDT, A. (2009). APT analyses of deuterium-loaded Fe/V multi-layered films. *Ultramicroscopy* **109**(5), 631-636.
- HALEY, D., MCCARROLL, I., BAGOT, P.A.J., CAIRNEY, J.M. & MOODY, M.P. (2019). A Gas-Phase Reaction Cell for Modern Atom Probe Systems. *Microscopy and Microanalysis* **25**(2), 410-417.
- HALEY, D., MERZLIKIN, S.V., CHOI, P. & RAABE, D. (2014). Atom probe tomography observation of hydrogen in high-Mn steel and silver charged via an electrolytic route. *International Journal of Hydrogen Energy* **39**(23), 12221-12229.
- JONATHAN BENNETT & AUTOIT TEAM. (2018). AutoIT. www.autoitscript.com. accessed: 12/6/19.
- KELLOGG, G.L. (1981). Pulsed laser stimulated field desorption of hydrogen from molybdenum. *The Journal of Chemical Physics* **74**(2), 1479-1487.
- KELLOGG, G.L. & PANITZ, J.K.G. (1980). A Direct observation of the Trapping of Deuterium Ions at a Grain Boundary in Tungsten. *Applied Physics Letters* **37**(7), 625-627.
- KELLOGG, G.L. & TSONG, T.T. (1980). Pulsed-Laser Atom-Probe Field-Ion Microscopy. *Journal of Applied Physics* **51**(2), 1184-1193.
- KESTEN, P., PUNDT, A., SCHMITZ, G., WEISHEIT, M., KREBS, H.U. & KIRCHHEIM, R. (2002). H- and D distribution in metallic multilayers studied by 3-dimensional atom probe analysis and secondary ion mass spectrometry. *Journal of Alloys and Compounds* **330**, 225-228.
- KOLLI, R.P. (2017). Controlling residual hydrogen gas in mass spectra during pulsed laser atom probe tomography. *Advanced Structural and Chemical Imaging* **3**(1), 10.
- KROM, A.H.M. & BAKKER, A. (2000). Hydrogen trapping models in steel. *Metallurgical and Materials Transactions B* **31**(6), 1475-1482.
- LIU, M.A., RIVERA-DÍAZ-DEL-CASTILLO, P.E.J., BARRAZA-FIERRO, J.I., CASTANEDA, H. & SRIVASTAVA, A. (2019). Microstructural influence on hydrogen permeation and trapping in steels. *Materials & Design* **167**, 107605.
- LONDON, A.J. (2019). Quantifying Uncertainty from Mass-Peak Overlaps in Atom Probe Microscopy. *Microscopy and Microanalysis* **25**(2), 378-388.
- MARIAN, J., HOANG, T., FLUSS, M. & HSIUNG, L.L. (2015). A review of helium-hydrogen synergistic effects in radiation damage observed in fusion energy steels and an interaction model to guide future understanding. *Journal of Nuclear Materials* **462**, 409-421.
- MARTIN, T.L., LONDON, A.J., JENKINS, B., HOPKIN, S.E., DOUGLAS, J.O., STYMAN, P.D., BAGOT, P.A.J. & MOODY, M.P. (2017). Comparing the Consistency of Atom Probe Tomography Measurements of Small-Scale Segregation and Clustering Between the LEAP 3000 and LEAP 5000 Instruments. *Microscopy and Microanalysis* **23**(2), 227-237.
- PROSA, T.J., GEISER, B.P., LAWRENCE, D., OLSON, D. & LARSON, D.J. Developing detection efficiency standards for atom probe tomography. In *Proc.SPIE*.
- REDDY, S.M., SAXEY, D.W., RICKARD, W.D.A., FOUGEROUSE, D., MONTALVO, S.D., VERBERNE, R. & VAN RIESSEN, A. (2020). Atom Probe Tomography: Development and Application to the Geosciences. *Geostandards and Geoanalytical Research* **44**(1), 5-50.
- ROBERTSON, I.M., SOFRONIS, P., NAGAO, A., MARTIN, M.L., WANG, S., GROSS, D.W. & NYGREN, K.E. (2015). Hydrogen Embrittlement Understood. *Metallurgical and Materials Transactions B-Process Metallurgy and Materials Processing Science* **46**(3), 1085-1103.
- RUSMAN, N.A.A. & DAHARI, M. (2016). A review on the current progress of metal hydrides material for solid-state hydrogen storage applications. *International Journal of Hydrogen Energy* **41**(28), 12108-12126.
- SUNDELL, G., THUVANDER, M. & ANDREN, H.O. (2013). Hydrogen analysis in APT: Methods to control adsorption and dissociation of H-2. *Ultramicroscopy* **132**, 285-289.

- TAKAHASHI, J., KAWAKAMI, K. & KOBAYASHI, Y. (2018). Origin of hydrogen trapping site in vanadium carbide precipitation strengthening steel. *Acta Materialia* **153**, 193-204.
- TAKAHASHI, J., KAWAKAMI, K., KOBAYASHI, Y. & TARUI, T. (2010). The first direct observation of hydrogen trapping sites in TiC precipitation-hardening steel through atom probe tomography. *Scripta Materialia* **63**(3), 261-264.
- TAKAHASHI, J., KAWAKAMI, K. & TARUI, T. (2012). Direct observation of hydrogen-trapping sites in vanadium carbide precipitation steel by atom probe tomography. *Scripta Materialia* **67**(2), 213-216.
- TSONG, T.T. (1978). Measurement of the field evaporation rate of several transition metals. *Journal of Physics F: Metal Physics* **8**(7), 1349-1352.

10. Tables

Table 1 *List of experiments using the Ratio method, including sample type and experimental sequence. Each named experiment family is for a single specimen.*

Name	Experiment Family	Experiment Type
Ratio-Low-Laser	Deuterium content estimation using Ratios, 0.2 nJ Laser	Pre-run, Voltage evaporation
		Pre-run, Laser evaporation
		Deuterated, Voltage evaporation
		Deuterated, Laser evaporation
Ratio-High-Laser	Deuterium content estimation using Ratios, 0.4 nJ Laser	Pre-run, Voltage evaporation
		Pre-run, Laser evaporation
		Deuterated, Voltage evaporation
		Deuterated, Laser evaporation

Table 2 List of experiments using the Extrapolation Method, including target detection and evaporation rates. Each named experiment family is for a single specimen.

Name	Experiment Family	Experiment Type	Target Detection Rate	Target Evaporation Rate	Frequency
Extrap-Manual	Deuterium content estimation using Extrapolation, manual experiments, 0.4 nJ Laser	Deuterated, laser evaporation	1 %	2.7 %	200 kHz
		Deuterated, laser evaporation	3.5 %	9.5 %	200 kHz
		Deuterated, laser evaporation	7 %	18.9 %	200 kHz
Extrap-Low-Rate	Hydrogen extrapolation, Low evaporation rate, 40 pJ Laser	Laser evaporation, automatic detection rate variation	0.1 %, 1 %, 10 %	0.125 %, 1.25 %, 12.5 %	200 kHz
Extrap-High-Rate	Hydrogen extrapolation, High evaporation rate, 40 pJ Laser	Laser evaporation, automatic detection rate variation	3 %, 8 %, 12 %	3.75 %, 10 %, 15 %	200 kHz
Extrap-Few-Step	Hydrogen extrapolation, low evaporation rate, reduced frequency of evaporation rate steps, 40 pJ Laser	Laser evaporation, automatic detection rate variation	0.07 %, 0.7 %, 7 %	0.125 %, 1.25 %, 12.5 %	200 kHz
Extrap-Freq-Few-Step	Hydrogen extrapolation, deuterated sample, 40 pJ Laser	Laser evaporation, automatic frequency variation	1 %	1.25 %	125 kHz, 250 kHz, 333 kHz
Extrap-Freq-Many-Step	Hydrogen extrapolation, deuterated sample, 40 pJ Laser	Laser evaporation, automatic frequency variation	1 %	1.25 %	125 kHz, 250 kHz, 333 kHz

Extending Estimating Hydrogen Content in APT

Extrap-Freq- High-Rate	Hydrogen extrapolation, high evaporation rate	Laser evaporation, automatic frequency variation	5.6 %	10 %	125 kHz, 250 kHz, 333 kHz
---------------------------	---	--	-------	------	---------------------------------

Table 3: Background-corrected ions counts in pulsed voltage- and laser experiments on vanadium carbide steel samples before and after deuteration (Ratio-Low-Laser and Ratio-High-Laser)

Experiment	Ratio-Low-Laser				Ratio-High-Laser			
	Voltage pre-run	Voltage deuterated	Laser 0.2 nJ pre-run	Laser 0.2 nJ deuterated	Voltage pre-run	Voltage, deuterated	Laser 0.4 nJ pre-run	Laser 0.4 nJ deuterated
Counts m/n= 1 Da	60	4033	2162	8216	371	1178	1684	14410
Counts m/n= 2 Da	No peak	4303	215	2601	No peak	531	331	5503
Total detector events	0.42M	47M	1.6M	7.8M	0.45M	1.1M	1.7M	7.7M

Table 4: Observed and expected detector events the location $m/n = 4$ Da

	Method	Ratio-Low-Laser	Ratio-High-Laser
		0.2 nJ Laser	0.4 nJ Laser
Observed Events	NA	123	92
Expected background noise events	fitted background	134	90
Expected D_2^+ events	H^+/H_2^+ ratio, using pre-run ratio	177	524

Table 5 Peak ratios and decomposition results for the ionic deuterium content in Ratio-Low-Laser and Ratio-High-Laser

Method		Sample 1 (Ratio-Low-Laser)	Sample 2 (Ratio-High-Laser)
H^+ / H_2^+ ratio in laser pre-run	Ratio of background-corrected peak heights (Table 3)	10.0	5.08
H^+ / H_2^+ ratio in deuterated laser run	Ratio of background-corrected peak heights (Table 3)	3.16	2.62
Estimated D^+ amount in deuterated laser run	Formula in section 2.1 for D^+ estimation	0.023 %	0.034 %
D^+ amount in deuterated voltage run	Amount of counts in m/n = 2 peak (noise-corrected)	0.009 %	0.046 %
Deviation of D^+ amount in laser run compared to voltage run	Relative deviation in percent	+ 256 %	- 74 %

11. Figure Legends

Figure 1: Illustration of a Hydrogen spectrum with Protium and Deuterium in APT (A) and the overlap problem upon H_2^+ molecule formation (B)

Figure 2: Spectra of paired samples before and after deuteration. A) pulsed voltage evaporation, Sample 1 (Ratio-Low-Laser) B) laser evaporation, 0.2nJ energy, Sample 1 (Ratio-Low-Laser) C) laser evaporation, 0.4 nJ energy, Sample 2 (Ratio-High-Laser). All Spectra are normalised to the sum of counts in the interval from 0 to 5 Da.

Figure 3: Ionic amounts of $m/n = 1,2$ Da (background corrected) as function of time between evaporation events t_E and linear extrapolation to $t_E = 0$ in a VC steel sample (Extrap-Manual), obtained in the sequential APT experiments on the same tip at different evaporation rates. R^2 values: 0.9996 ($m/n = 1$ Da), 0.914 ($m/n = 2$ Da)

Figure 4: Background corrected ionic amounts of combined FeH_2^+ and FeD^+ , FeH^+ and FeD_2^+ and linear extrapolation to zero time between evaporation events in a vanadium carbide steel sample. R^2 values: 0.986 ($FeH_2^+ + FeD^+$), 0.991 (FeH^+), 0.995 (FeD_2^+).

Figure 5: Sections of evaporation rate and hydrogen concentration evolution from the automatically cycled evaporation rate experiments at low rate (Extrap-Low-Rate, A), high-rate (Extrap-High-Rate, B) and low rate with less frequent steps (Extrap-Few-Step, C). H_3^+ ions were observed in Extrap-Low-Rate only. Note that X-axis values are offset, i.e. do not correspond to the absolute ion numbers during the experiments. It is seen that the hydrogen content in A and C gradually tails off after phases with low detection rate, while no similar tail-off is observed in B. The short spikes in H^+ and H_2^+ in C are due to laser focus events to maintain sample tracking. The outlined/filled rectangles below the axes in C indicate the data recorded within 100000 detector events before/after evaporation rate changes

Figure 6: Detected ionic fractions of hydrogen as function of time between evaporation events t_E for the low-rate extrapolation experiment (Extrap-Low-Rate, A) and the high-rate extrapolation experiment (Extrap-High-Rate, B). R^2 values: 0.9695 (A), > 0.9999 (B)

Figure 7: Detected ionic amounts of hydrogen as function of time between evaporation events t_E for Extrap-Few-Step. Data shown for entire dataset (A), only the first 100000 detector events after each change in target evaporation rate (B), and only the last 100000 detector events before each change in target evaporation rate (C). Increased linearity suggests step-transitions account for much of the observed non-linearity.

Figure 8: Detected ionic fractions of hydrogen as function of time between evaporation events t_E for the cycled frequency experiments Extrap-Freq-Few-Step (A), Extrap-Freq-Many-Step (B) and Extrap-Freq-High-Rate (C). It is seen that the hydrogen content evolves relatively linear with the evaporation time t_E in all experiments, however a deviation similar to Extrap-Lpow-Rate is seen in Extrap-Freq-Few-Step. R^2 values: 0.9829 (A), 0.9990 (B), 0.9993 (C).

Figure 9: Depth profiles of extrapolated hydrogen in Extrap-Low-Rate (A), Extrap-High-Rate (B), Extrap-Freq-Few-Step and Extrap-Freq-Many-Step (C) and Extrap-Freq-High-Rate (D). The dots in the diagrams correspond to extrapolated values for each layer, and the lines show moving averages across the layers.

Figure 10: Voxel-based extrapolation of H^+ and H_2^+ in Extrap-Freq-High-Rate. A region of increased H^+ content is seen on the top of the tip, possibly corresponding to a surface oxide.

12. Figures

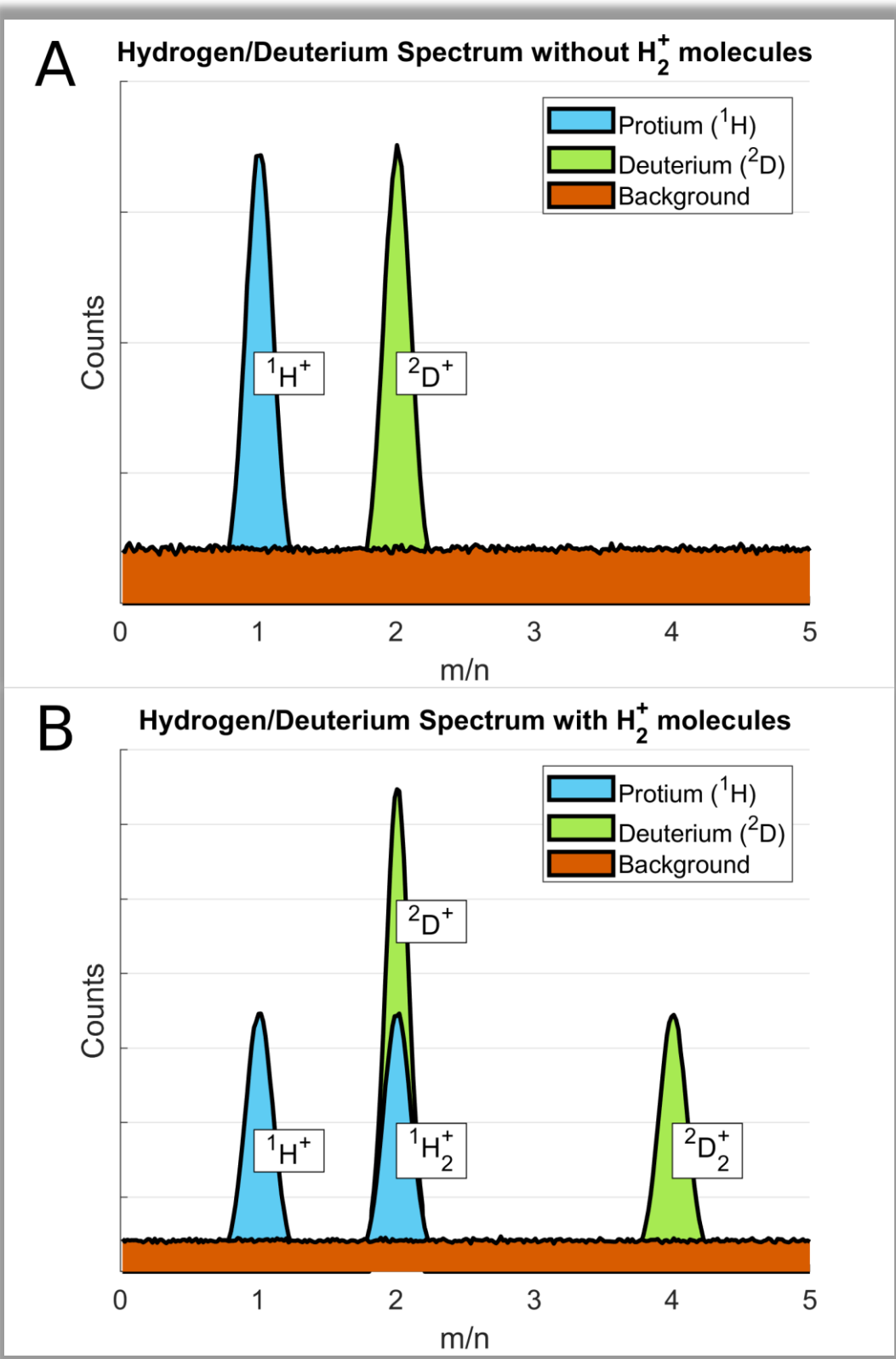


Figure 1

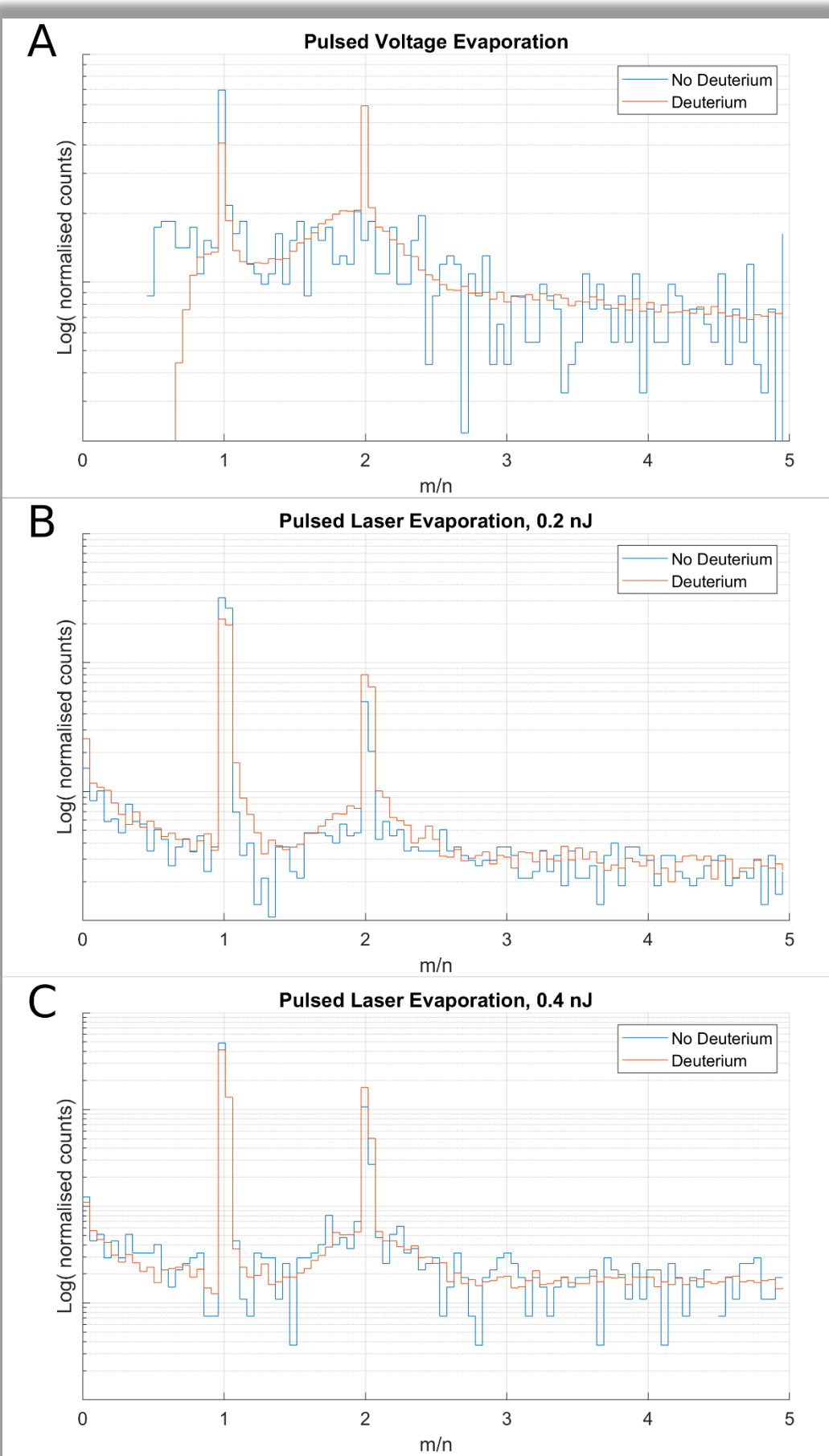


Figure 2

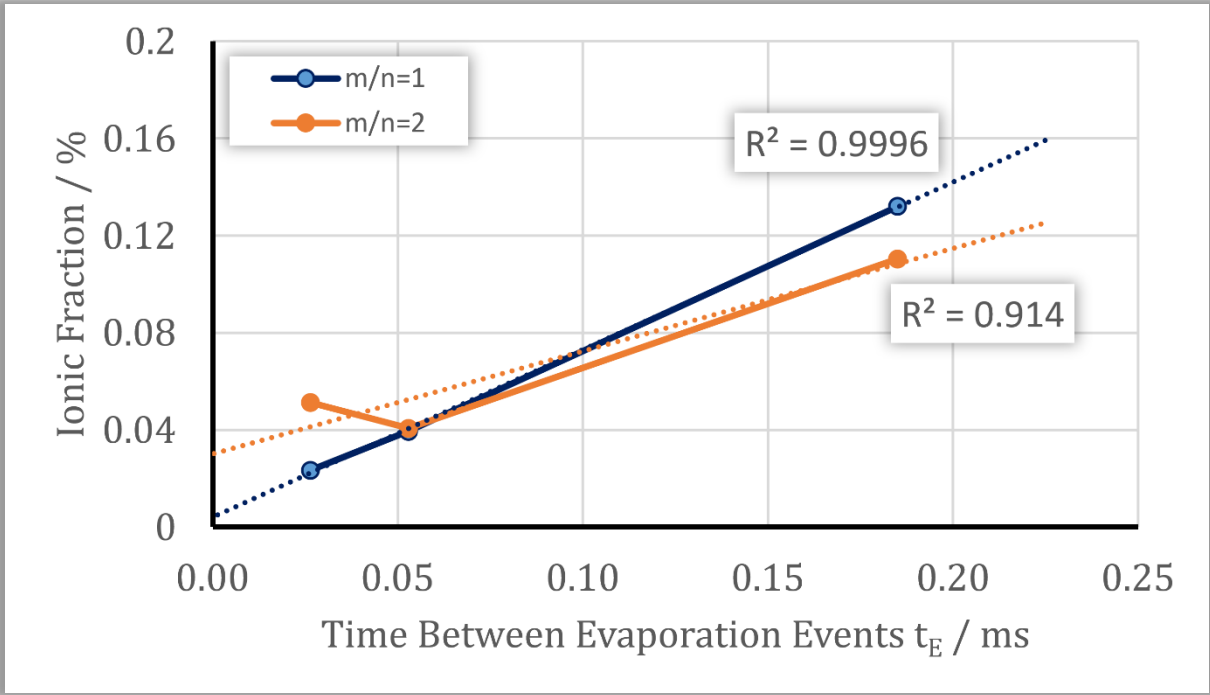


Figure 3

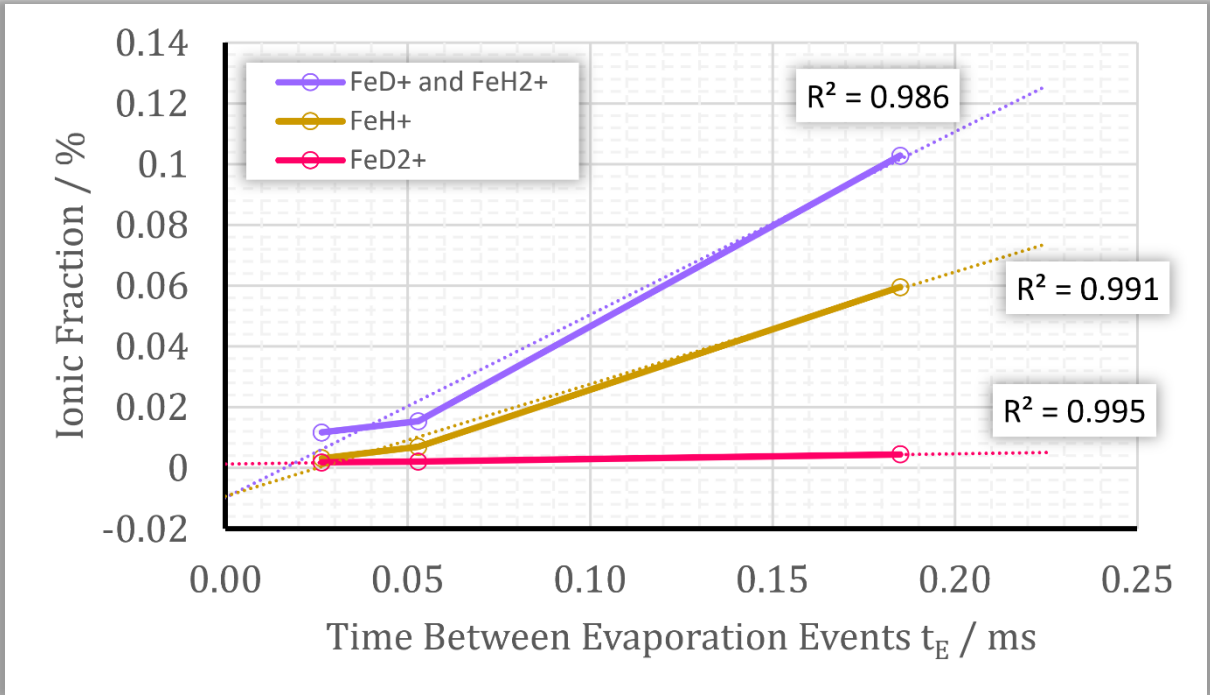


Figure 4

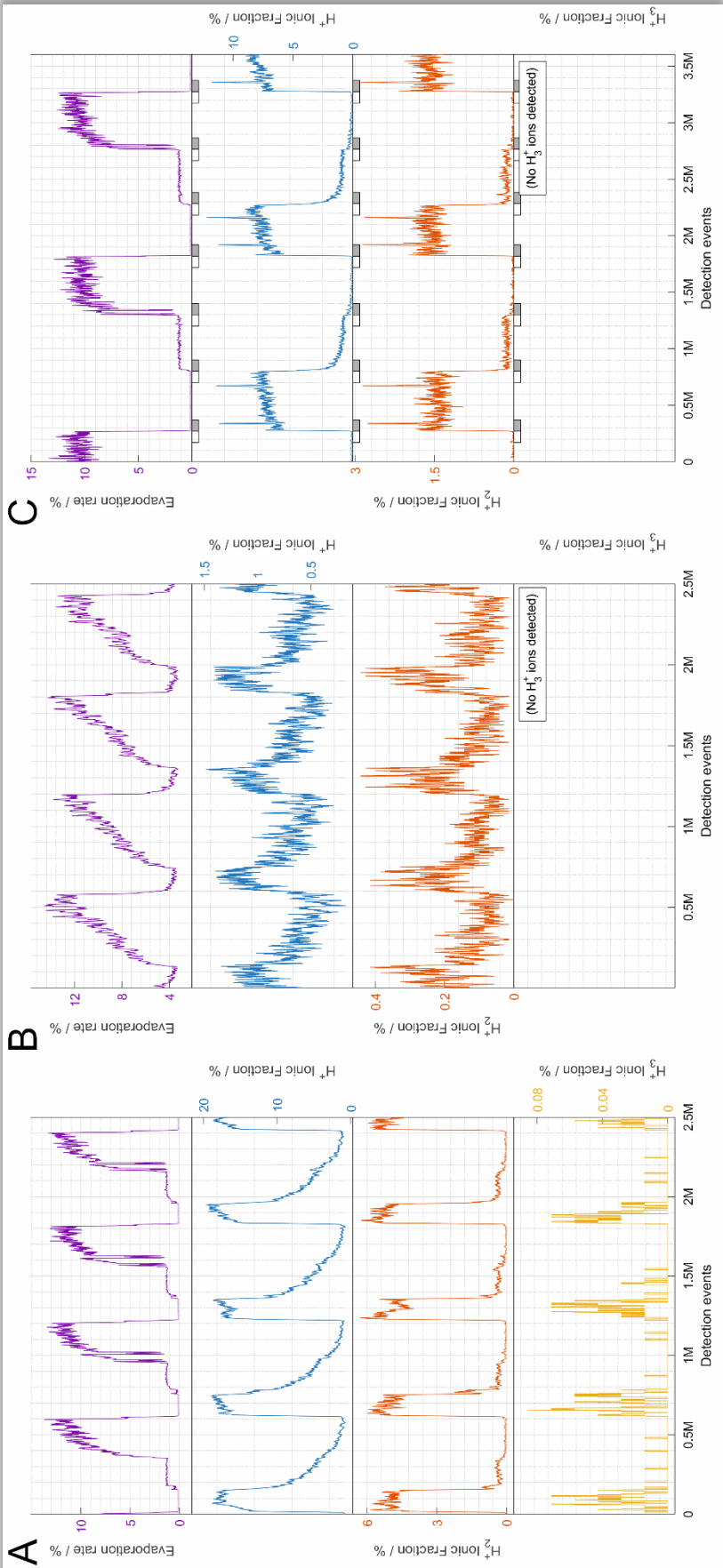


Figure 5

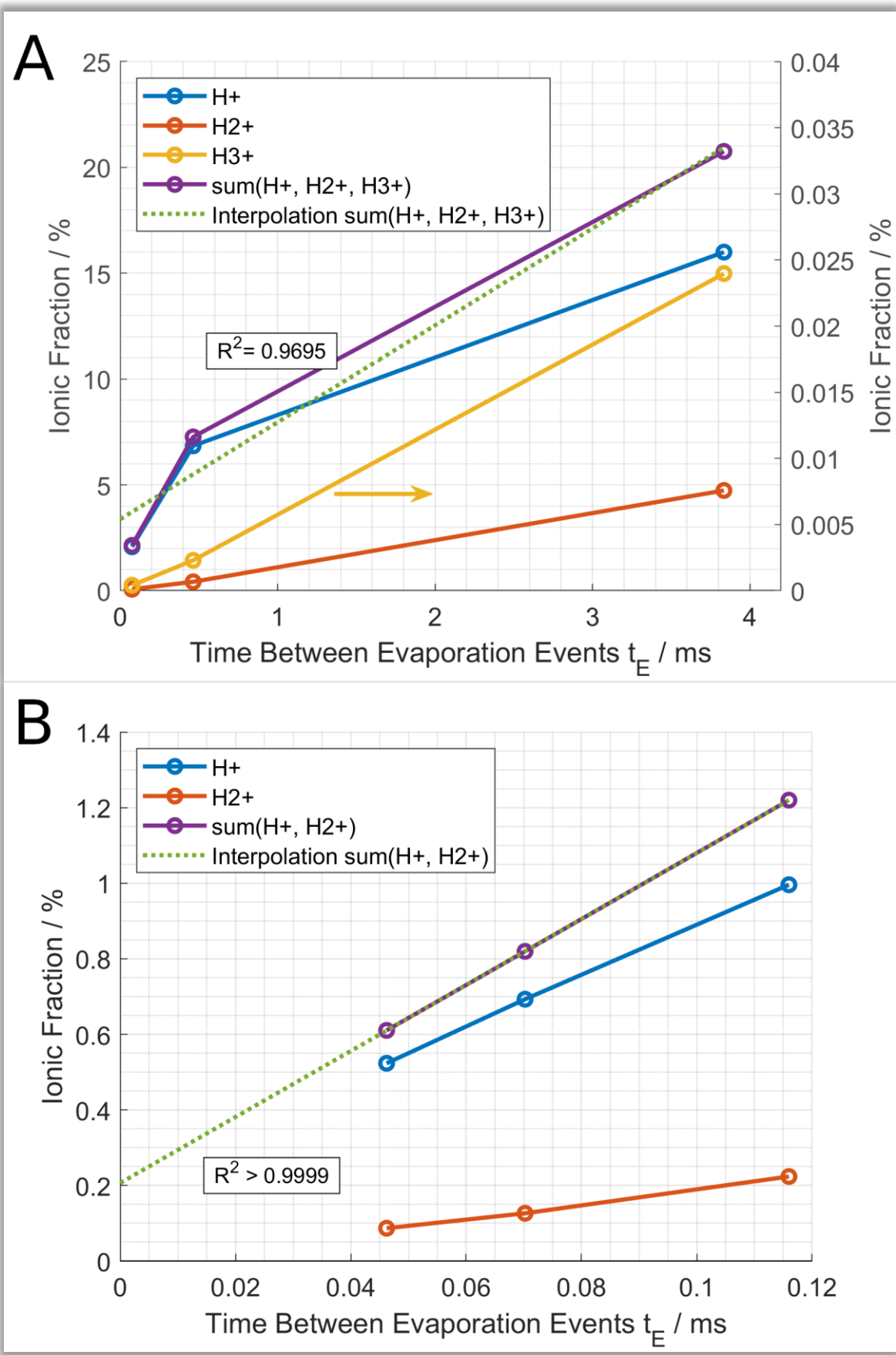


Figure 6

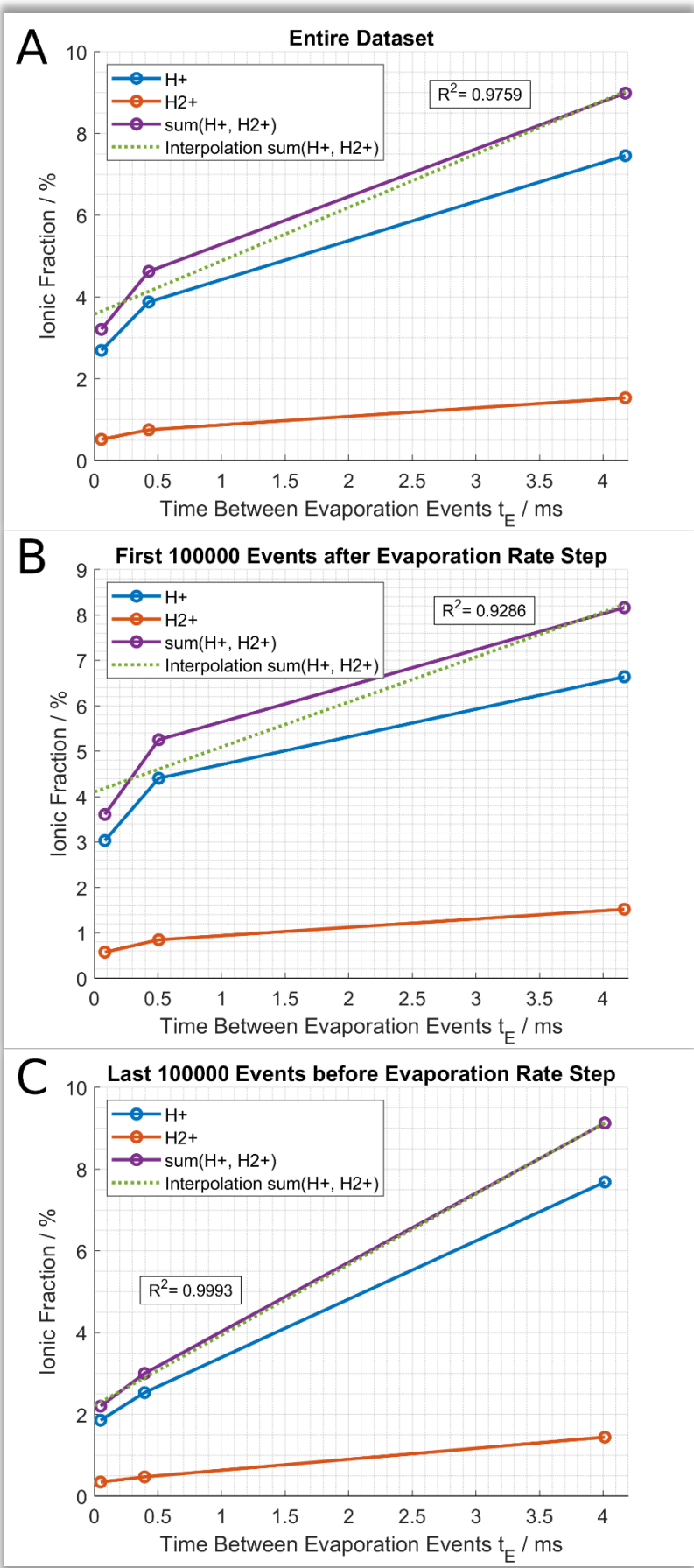


Figure 7

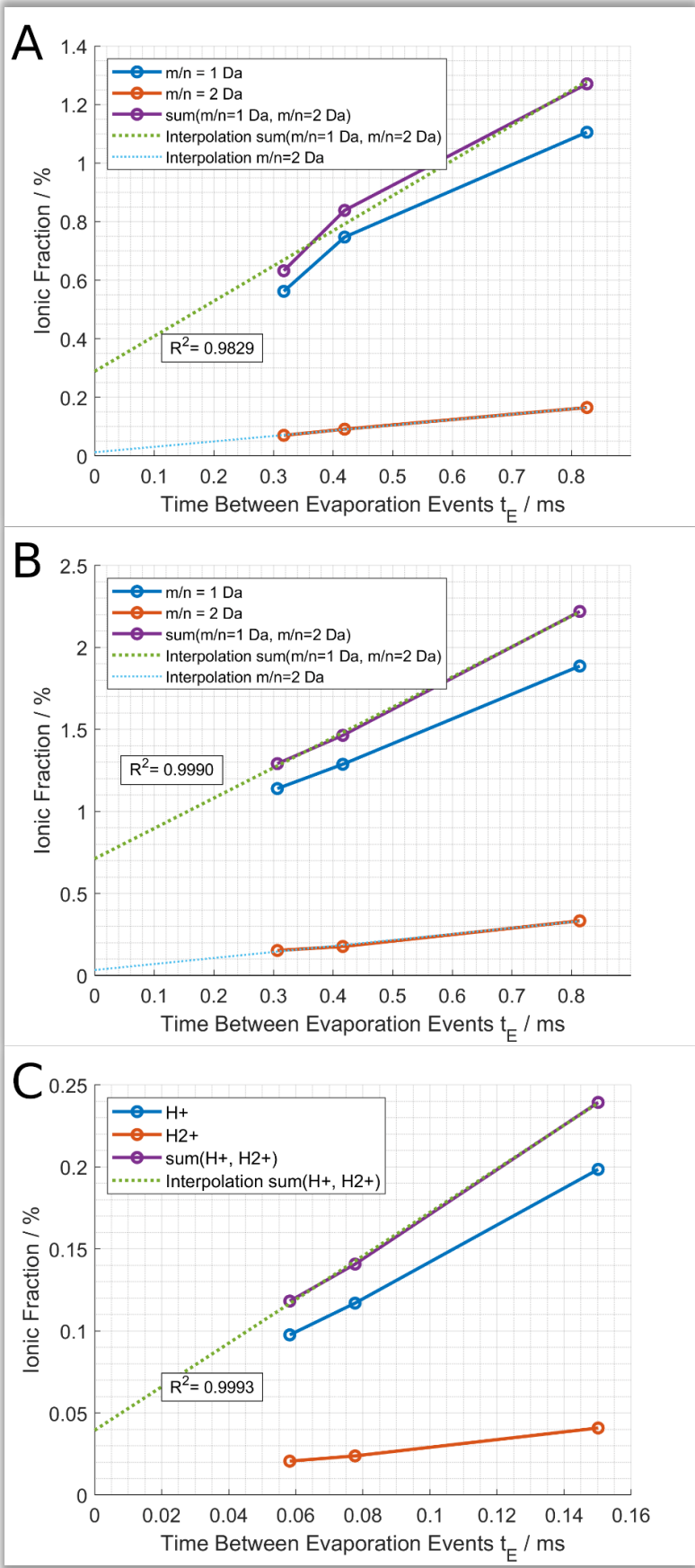


Figure 8

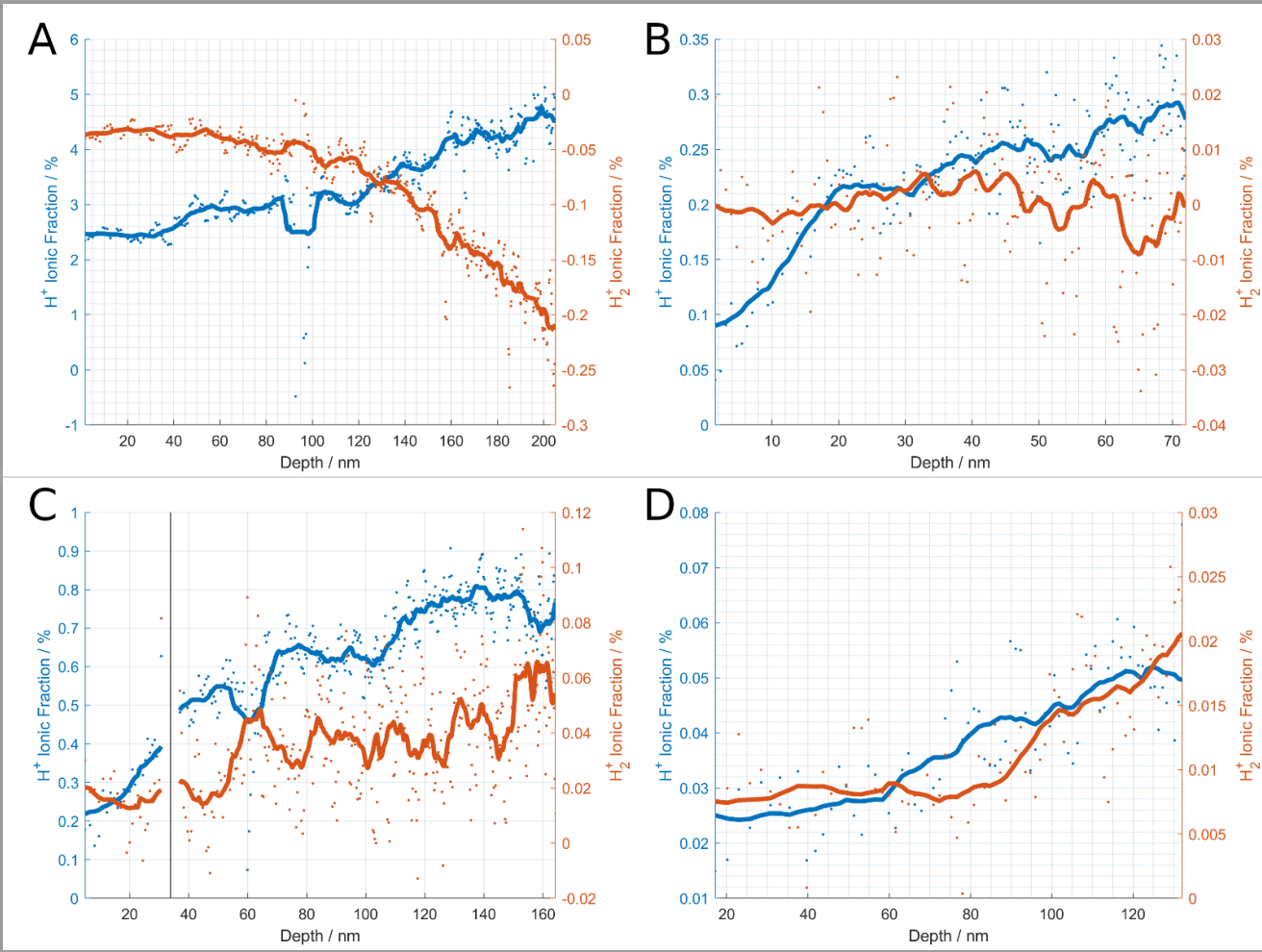


Figure 9

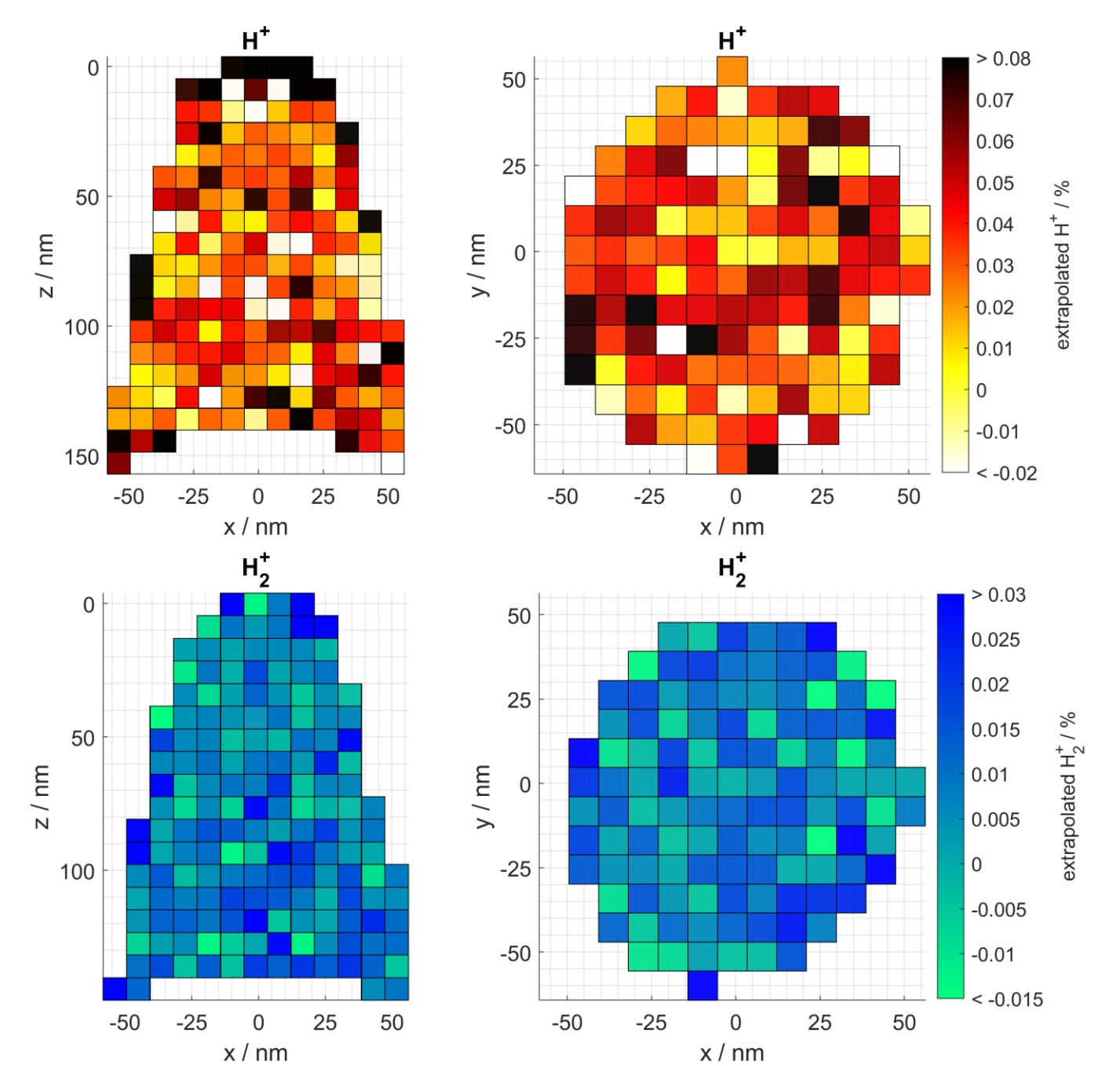


Figure 10